Simple self-shadowing in precise orbit determination of Copernicus Sentinel satellites

EGU23-13569
European Geosciences Union
General Assembly 2023
23 - 28 April 2023, Vienna, Austria

D. Arnold[1], H. Peter[2], A. Jäggi[1]

[1]Astronomical Institute, University of Bern, Bern, Switzerland
[2]PosiTim UG, Seeheim-Jugenheim, Germany

Introduction

- To model **non-gravitational accelerations (NGAs)** acting on a satellite in low Earth orbit – due to direct solar radiation pressure (SRP), visual and infrared planetary radiation pressure (PRP) and gas-surface interactions (drag) – the area to mass ratios A/m of satellite surface elements are needed.
- Often, the explicit NGA modeling is based on a simple **satellite macro model**, i.e., a geometry composed of a number of elementary shapes like flat plates, spheres or cylinders, each of which with a specific size, orientation and surface property. In a first approximation, each elementary surface is treated fully independent from the other surfaces and the (partial) occultation or shadowing of one surface by other surfaces is neglected. This can lead to degradations of NGA modeling for satellites with significant **non-convex shapes**.
- Very detailed satellite geometry models together with techniques like ray tracing can provide highly accurate NGAs, however, at the price of computational time and complexity.
- If the satellite is described by a set of flat convex polygons, for each plate the amount of shadow cast by the other plates can be computed analytically in a relatively straightforward way. We present the algorithm and first test results to assess its performance for POD.

The self-shadowing algorithm

The algorithm assumes that the shadow casting or receiving surface elements are all **convex flat polygons**. Notice that all (also non-convex) shapes can be composed out of convex polygons.

Input:

- Node (vertex) coordinates in the satellite body frame (SBF).
- A direction unit vector $\vec{d}$ associated to the NGA source (e.g., direction Sun-satellite for SRP modeling).

Initialization:

- Node coordinates are stored and checked to form flat convex polygons, ordered in counter-clockwise sense when watching from outside (defined by normal vector).
- For each plate i the basis vectors of the associated plate frame (PF_i) are computed and stored. The PF is defined as follows: Origin in 1st node, x-axis in direction from 1st to 2nd node, z-axis in outgoing normal direction, y-axis completing right-handed orthogonal system.
- For each non-moving plate i, the node coordinates of all other non-moving plates in PF_i are computed and stored. For moving plates (e.g., rotating solar panels) the PF coordinates need to be computed at every integration step based on the current plate orientation.

At each satellite orbit integration step, when NGAs are evaluated, for each individual plate R (shadow receiving plate) which is exposed to the source (ignoring the other plates) the following algorithm is executed for each other plate C_i (shadow casting plate):

1. Check whether plate C_i is exposed to source. If yes, skip it, because it cannot cast a shadow (it is then the back side of C_i which might cast a shadow).
2. Transform node coordinates of C_i into PF_R (either reading them from memory or computing them using the momentary PF_R basis vectors). Do all following computations in PF_R.

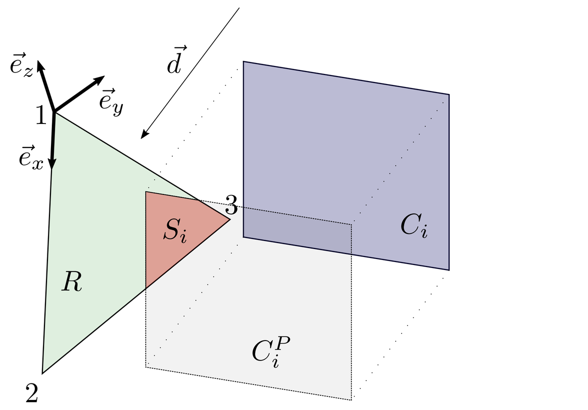

Figure 1: The shadow receiving plate R with basis vectors of PF_R, a shadow casting plate C_i, its projection C_i^P along $\vec{d}$ onto the plane of R and the resulting shadow S_i on R.

3. Count how many nodes of C_i are in front of R (i.e., have a positive PF_R z-coordinate).
   (a) If none, skip C_i, as it cannot cast a shadow onto R.
   (b) If all, go to step 4.
   (c) If part of them, clip the polygon C_i to the part in front of R. Do this by computing the intersection points of the edges of C_i with the plane of plate R. Add them and drop all nodes behind R.
4. Compute projection of nodes of (clipped) polygon C_i onto the plane of plate R in the direction of $\vec{d}$. This results in another convex polygon C_i^P.
5. Find the (convex) overlapping polygon $S_i = C_i^P \cap R$. Do this by clipping C_i^P to R using, e.g., the Sutherland-Hodgman polygon clipping algorithm. Compute the area $A(S_i)$ of the overlap (using shoelace formula).
   (a) If $A(S_i) = 0$ (shadow polygon C_i^P entirely outside R), skip C_i.
   (b) If $A(S_i) = A(R)$ (the area of R), stop the algorithm as R is fully shadowed by C_i.
   (c) If $0 < A(S_i) < A(R)$, store nodes of S_i and $A(S_i)$ in a list `lst`. Give $A(S_i)$ a negative sign.
6. Compute overlap of S_i with all other (convex) polygons L_j previously stored in `lst`, again using, e.g., the Sutherland-Hodgman polygon clipping algorithm. Store these (convex) overlap polygons $S_i \cap L_j$ and their areas $A(S_i \cap L_j)$ also in `lst`. Set the sign of $A(S_i \cap L_j)$ to the negative of the sign of $A(L_j)$.

After repeating these 6 steps for all plates C_i, the non-shadowed area of R can now be computed by adding all $A(L_j)$ in `lst` to $A(R)$. This implements the inclusion-exclusion principle, according to which the area of the union of all n shadow polygons S_i on R is given by

$$A\left(\bigcup_{i=1}^{n} S_i\right) = \sum_{k=1}^{n}\left((-1)^{k+1} \sum_{1 \le i_1 < \ldots < i_k \le n} A\left(S_{i_1} \cap \ldots \cap S_{i_k}\right)\right),$$

and which takes into account the overlap of shadows of different plates on R (avoiding double counting of shaded areas).

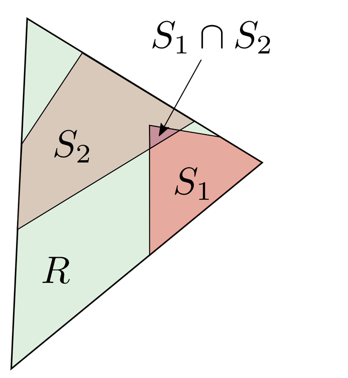

Figure 2: Shadow receiving plate R with two overlapping (convex) shadow polygons S_1 and S_2. The non-shadowed area of R equals $A(R) - A(S_1) - A(S_2) + A(S_1 \cap S_2)$.

Application to Sentinel-1

The above self-shadowing algorithm was implemented into the Bernese GNSS Software and used for POD tests of the Copernicus Sentinel-1A satellite (about 700 km altitude).

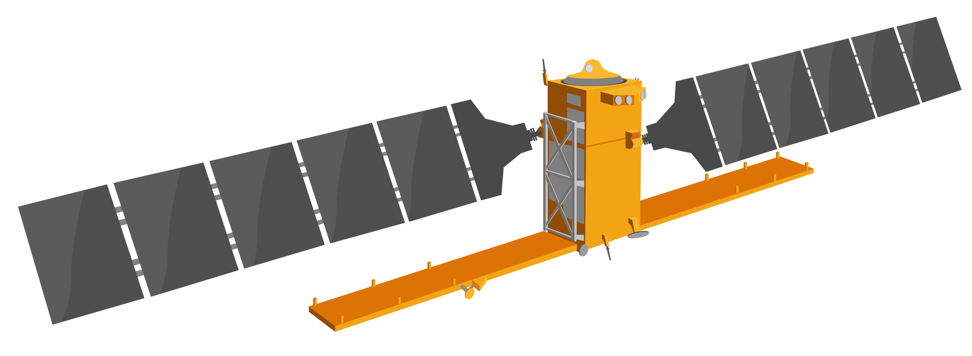

Figure 3: Sentinel-1 satellite with large SAR antenna on the bottom (image from https://blogs.fu-berlin.de/reseda/sentinel-1). The SBF has its origin in the center on top, the x-axis points into the direction of the left solar panel axis (flight direction) and z down towards the SAR antenna. The right solar panel can cast a significant shadow onto the back side of the SAR antenna.

The "standard" Sentinel-1 macro model (proposed by the Copernicus POD Service) consists of 8 flat plates, modeling the satellite bus, SAR antenna and solar panels (Peter et al., 2020).

Peter et al. (2020) have proposed a simple adjustment of three plates of the standard Sentinel-1 macro model depending on the solar incidence angle to take the following self-shadowings for direct SRP into account: Right SAR antenna back side by right solar panel, $-x$ body side by right solar panel and left solar panel by body.

For the present study, a 14-plate macro model with separate plates for the bus $-z$ plate, the two back sides of the SAR antenna, separate plates for the front and back solar panels, and the long SAR antenna side plates is used. Figure 4 compares the shadowed area of the right ($-x$) SAR antenna back side following Peter et al. (2020) and using the presented self-shadowing algorithm.

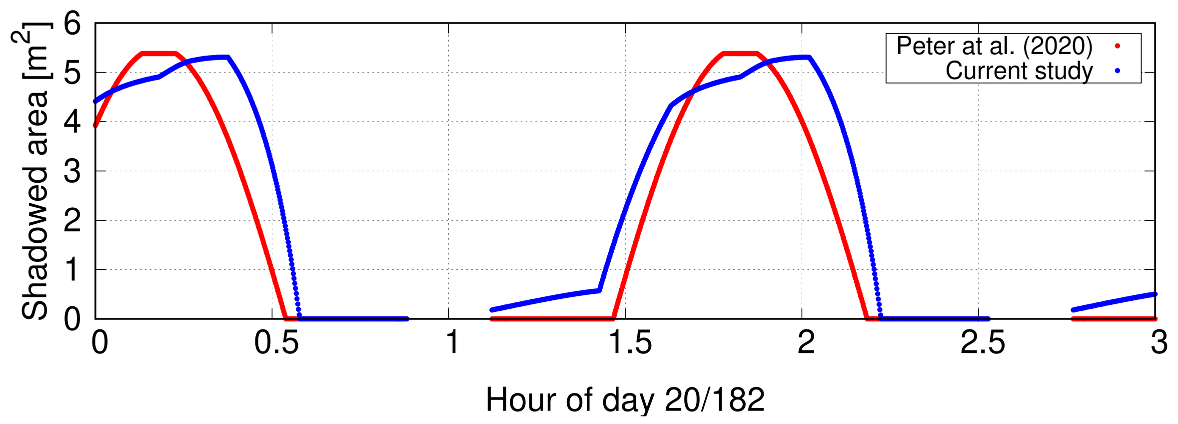

Figure 4: Shadowed area of right back side of Sentinel-1A SAR antenna for the first three hours of June 30, 2020 ($\beta_{\mathrm{Sun}} = 58.7°$). Red: Peter et al. (2020) only consider shadowing due to the right solar panel and assume Sun incidence perpendicular to x-direction. Blue: The presented self-shadowing algorithm uses the true Sun incidence angle and also detects shadowing by the $-x$ bus plate (max. 0.6 m^2 in this example).

The next largest shadowings, which are detected by the proposed algorithm and which are neglected in Peter et al. (2020) are: $-y$ side of SAR antenna by right solar array (max. 0.9 m^2), as well as both SAR antenna back sides by body (max. 0.6 m^2 each).

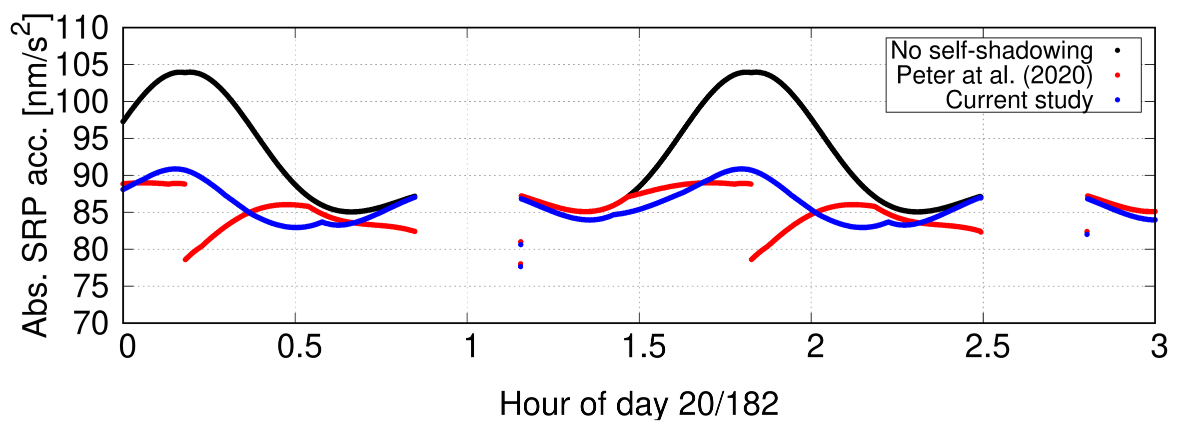

Figure 5: Magnitude of total acceleration due to direct SRP for Sentinel-1A when taking no self-shadowing into account (black), when modeling self-shadowing as in Peter et al. (2020) (red), or when using the proposed algorithm (blue). The jumps in the red curve are due to an erroneously modeled shadowing of the left solar panel.

To compare the impact of the self-shadowing handling strategies for POD, Sentinel-1A orbits were computed for the time period January 1 - August 31, 2022. The 24 h arc-wise estimated orbit parameters constitute osculating orbital elements, 1/rev empirical accelerations in radial, along-track and cross-track direction, and 1 SRP and 1 air drag scaling factor. Figure 6 shows that the estimated empirical accelerations tend to become smaller, especially in cross-track, if self-shadowing is considered.

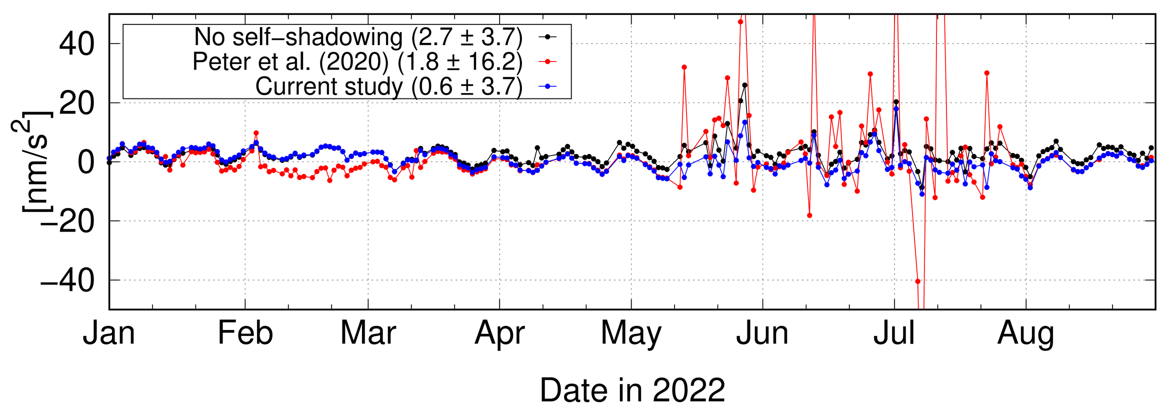

Figure 6: Estimated cross-track 1/rev sine accelerations. Between May 14 and July 30, 2022 the satellite has its eclipse period.

Application to Sentinel-6

Sentinel-6A (about 1340 km altitude) is another example for a satellite of marked non-convex shape, implying significant self-shadowing especially between the body side panels and the overhanging deployable solar panels (DSP). Several Sentinel-6 macro models exist, part of them aim to take self-shadowing into account (e.g., by reducing the areas of the body side panels).

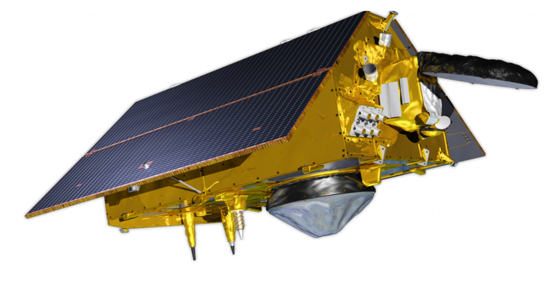

Figure 7: The altimetry satellite Sentinel-6 Michael Freilich. Flight direction ($+x$) is towards tilted microwave antenna on the right, $+z$ downwards. Credits: NASA

The following models were tested: MOD1: 12-plate model of the Sentinel-6 POD Context document (v2.1) with body $\pm y$ areas 2.87 m^2. MOD2: Like MOD1, but with areas of body $\pm y$ side panels reduced to 1.03 m^2. MOD3: 6-plate model of CNES with adapted optical properties, presented at Copernicus POD Quality Working Group meeting #11.

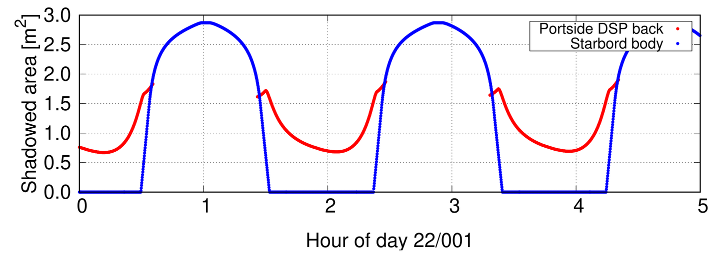

Figure 8: Shadowing of portside DSP backside by satellite body (red) and starbord body side by starbord DSP backside (blue) for the first five hours of January 1st, 2022 ($\beta_{\mathrm{Sun}} = -13.1°$). MOD1 and the proposed algorithm were used.

The different macro models were used for POD tests based on the identical orbit parametrization as for Sentinel-1. Figure 9 shows that for Sentinel-6 the employed self-shadowing handling does not yet provide convincing results. Further macro model modifications must be tested.

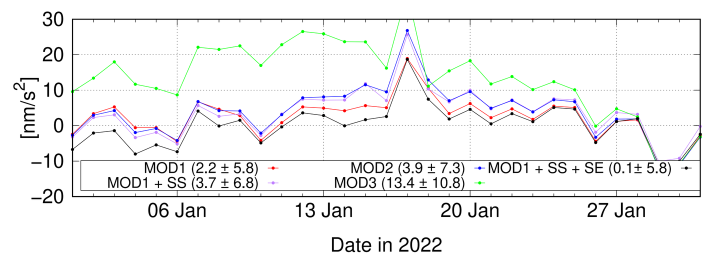

Figure 9: Estimated radial 1/rev cosine accelerations. The purple values were obtained with the proposed self-shadowing (SS) algorithm. The black values result, if spontaneous re-emission (SE) for the solar panels is deactivated.

Computation time

For Sentinel-1, the use of a 14-plate instead of an 8-plate macro model (still without self-shadowing handling) increased CPU time for an orbit integration by 34 %. For both Sentinel-1 and Sentinel-6, switching on the self-shadowing algorithm (only for direct SRP) caused only an insignificant increase of CPU time (below 1 %).

The proposed self-shadowing algorithm can very easily also be employed in the modeling of planetary radiation pressure (PRP) or air drag (using the associated vector for $\vec{d}$). For PRP computations based on Earth radiation grids this can be computationally expensive, depending on the desired self-shadowing resolution.

Conclusions

The presented algorithm can be used to flexibly model self-shadowing effects for a satellite macro model composed of convex plate elements. For the analyzed geometries the algorithm is very efficient, but is expected to become more expensive for much more complex geometries (including multiple shadow overlaps). The impact on POD results is so far marginal, or, in case of Sentinel-6, even slightly detrimental. Further investigations are needed to analyze more precise geometries and optical surface properties.

References

Peter, H., Fernández, J., and Féménias, P. (2020). Copernicus Sentinel-1 satellites: sensitivity of antenna offset estimation to orbit and observation modelling. *Advances in Geosciences*, 50:87–100.

Contact address

Daniel Arnold
Astronomical Institute, University of Bern
Sidlerstrasse 5
3012 Bern (Switzerland)
daniel.arnold@unibe.ch

Sharing is encouraged

Poster compiled by Daniel Arnold, April 2023
Astronomical Institute, University of Bern, Bern
daniel.arnold@unibe.ch